Journal of the Ceramic Society of Japan 125 [4] 236-241 2017 **Full paper**

Characteristics of $La_{0.8}Sr_{0.2}Ga_{0.8}Mg_{0.2}O_{3-\delta}$-supported micro-tubular solid oxide fuel cells with bi-layer and tri-layer electrolytes

Yi-Xin LIU, Sea-Fue WANG†, Yung-Fu HSU and Piotr JASINSKI*

Department of Materials and Mineral Resources Engineering, National Taipei University of Technology, Taipei 106, Taiwan
***Faculty of Electronics, Telecommunications and Informatics, Gdańsk University of Technology, Gdansk, Poland**

In this study, $La_{0.8}Sr_{0.2}Ga_{0.8}Mg_{0.2}O_{3-\delta}$ (LSGM)-supported micro tubular solid oxide fuel cells (T-SOFCs) with two different configurations, one containing an LSGM–$Ce_{0.6}La_{0.4}O_{2-\delta}$ (LDC) bi-layer electrolyte (Cell A) and one containing an LDC–LSGM–LDC tri-layer electrolyte (Cell B), were fabricated using extrusion and dip-coating. After optimizing the paste formulation for extrusion, the flexural strength of the dense and uniform LSGM micro-tubes sintered at 1500°C was determined to be approximately 144 MPa. Owing to the insertion of an LDC layer between LSGM electrolyte and $La_{0.6}Sr_{0.4}Co_{0.2}Fe_{0.8}O_{3-\delta}$ (LSCF)–LSGM cathode, the ohmic resistances of Cell B were slightly larger than those of Cell A at the operating temperatures investigated, mainly because of interfacial resistance, but Cell B exhibited slightly lower polarization resistance than Cell A. The maximum power densities (MPDs) of Cell A were 0.25, 0.35, 0.43, and 0.47 $W\,cm^{-2}$ at 650, 700, 750, and 800°C, respectively, which are slightly larger than those of Cell B, i.e., 0.23, 0.33, 0.42, and 0.41 $W\,cm^{-2}$, respectively, owing to the facts that Cell A exhibited a slightly higher open-circuit voltage and a smaller R_t value. Cell A containing the LSGM (288 μm)–LDC (8 μm) bi-layer electrolyte can be operated at approximately 650°C with an MPD value of approximately 0.25 $W\,cm^{-2}$; however, a similarly structured single cell containing a $Zr_{0.8}Sc_{0.2}O_{2-\delta}$ (ScSZ) (210 μm) electrolyte need to be operated at 900°C, and one containing an $Ce_{0.8}Gd_{0.2}O_{2-\delta}$ (GDC; 285 μm)–ScSZ (8 μm) bi-layer electrolyte has to be operated at 700°C. Thus, the advantage of using LSGM as an electrolyte for micro T-SOFC single cells is apparent.

Key-words : Solid oxide fuel cell, Tubular, Extrusion, Dip-coating, Sintering, LSGM

[Received October 30, 2016; Accepted January 19, 2017]

1. Introduction

Solid oxide fuel cells (SOFCs) have attracted interest worldwide for their commercialization potential owing to their high-energy conversion efficiency, low pollutant emission, excellent fuel flexibility, and non-reliance on noble metals for their electrodes.1) SOFCs with several different configurations, including planar, monolithic, and tubular designs, have been developed. Compared to other configurations, tubular SOFCs exhibit excellent thermal resistance, secure sealing, solid mechanical strength, rapid heat cycling, and stable performance at high temperatures (700–1000°C).2)–4) The fabrication of tubular SOFCs (T-SOFCs) usually involves tube formation and layer deposition steps. Ceramic micro-tubes can be prepared using extrusion, gel casting, isostatic pressing, or phase inversion methods, while further layer deposition methods include dip-coating, plating, electrophoretic deposition, and spray-coating.5)–10) The drawbacks of tubular SOFCs are their low current density and complexity of fabrication.4) Accordingly, considerable research effort has been invested in reducing cell size and fabricating anode-supported SOFCs with thin electrolytes for improved volumetric power density.7) However, anode-supported T-SOFCs are prone to mechanical failure during operation, which is caused primarily by the significant volume change (around 40 vol.%) in the anode layer during reduction and re-oxidation cycles. This volume change can lead to cracking of the thin electrolyte layer and delamination of the electrode and electrolyte layers.8),11) The electrolyte-supported design is generally regarded to be more stable than its anode-supported counterpart.

A previous study, in which extrusion and dip coating were used to prepare electrolyte-supported micro T-SOFCs, revealed that NiO/NiO–$Zr_{0.8}Sc_{0.2}O_{2-\delta}$ (ScSZ)/ScSZ/$Ce_{0.8}Gd_{0.2}O_{2-\delta}$ (GDC)–$La_{1-x}Sx_rMnO_{3-\delta}$ (LSM) cell exhibited a good flexural strength (190 MPa). Furthermore, the micro T-SOFCs showed no delamination after thermal recycling and retained good mechanical integrity.6) However, the maximum power density (MPD) of the micro T-SOFCs reached only 0.23 $W\,cm^{-2}$ at 900°C owing to the high ohmic and polarization resistances of the cells. The ohmic resistance can be decreased by using $Ce_{0.8}Sm_{0.2}O_{2-\delta}$ (SDC) as the electrolyte, which further helps to lower the operating temperature.12),13) However, the cell performance may be diminished by the poor mechanical strength and electronic conduction of the electrolyte. It has been shown that Ce^{4+} ions can be reduced to Ce^{3+} ions under a reducing atmosphere, thereby causing some electronic conduction in the electrolyte, resulting in the drop of open-circuit voltage (OCV).14) These problems can be overcome by the use of alternative electrolytes that have higher ionic conductivities at low temperatures, such as $La_{0.8}Sr_{0.2}Ga_{0.8}Mg_{0.2}O_{3-\delta}$ (LSGM). LSGM materials have superior oxygen ion conductivity, typically 0.17 $S\,cm^{-1}$ at 800°C and 0.034 $S\,cm^{-1}$ at 600°C, negligible electronic conduction, and high chemical stability over a broad range of oxygen partial pressures (1×10^{-15} to 1×10^{5} Pa), making them a promising electrolyte material in the form of intermediate temperature SOFCs (IT-SOFCs).15) As reported for studies on planar SOFC single cells, Yu et al. and Bozza

---

† Corresponding author: S.-F. Wang; E-mail: sfwang@ntut.edu.tw

‡ Preface for this article: DOI http://doi.org/10.2109/jcersj2.125.P4-1

DOI http://doi.org/10.2109/jcersj2.16244

Table 1. Formulations of electrolyte pastes and characteristics of extruded green micro-tubes

Sample No.	Additives				Characteristics of the green micro-tubes
	MC (wt%)	Oil (wt%)	D.I. Water (wt%)	Surfactant. (wt%)	
LSGM-1	0.92	1.33	13.72	0.47	Worm shape, not smooth to extrude
LSGM-2	1.17	1.33	13.74	0.50	Good shape, smooth surface
LSGM-3	1.27	1.33	13.72	0.50	Good shape, low green density
LSGM-4	1.17	1.25	13.75	0.50	Rough surface, not easy to extrude
LSGM-5	1.16	1.46	13.72	0.50	Pinholes on surface, tube elongated
LSGM-6	1.17	1.33	13.76	0.33	Dry paste, not extrudable
LSGM-7	1.16	1.33	13.70	0.75	Good shape, smooth surface

et al.18),29),30) inserted a $Ce_{0.6}La_{0.4}O_2$ (LDC) layer between an LSGM electrolyte and NiO anode to prevent the chemical reaction between LSGM and NiO during sintering,21) while Lin et al. and Wan et al.27),31) introduced LDC between an LSGM electrolyte and both electrodes to improve the cell characteristics. However, direct comparisons of SOFCs with insertion of LDC between LSGM electrolyte and anode and those with introduction of LDC between LSGM electrolyte and both electrodes have never been reported in the literature. There are also very few reports in the literature regarding T-SOFCs with LSGM electrolytes, and these reports have focused either on anode-supported SOFCs with dip-coated and electrophoretically deposited thin LSGM electrolytes,16)–18) or on electrolyte-supported SOFCs with dip-coated or extruded LSGM tubes.19),20) The former T-SOFCs exhibit high power densities, but have problems with long-term stability. The latter T-SOFCs exhibit inferior power densities and property degradation owing to inter-diffusion of the species between the different layers.

The goals of this study were to explore the processing conditions of the T-SOFCs with extruded LSGM electrolyte as mechanical support and with dip-coated NiO and LSCF electrodes, to incorporate LDC as buffer layer that has been used in planar SOFCs, and to compare the cell properties of SOFCs with a LDC layer inserted between LSGM electrolyte and anode and those with two LDC layers introduced between LSGM electrolyte and both electrodes. Two different electrolyte-supported micro T-SOFCs with different electrolyte configurations were developed in this study based on LSGM electrolytes, Ni anodes, and $La_{0.6}Sr_{0.4}Co_{0.2}Fe_{0.8}O_{3-\delta}$ (LSCF) cathodes. The first configuration incorporates a buffer layer of LDC, an LSCF–LSGM composite cathode, and a bi-layer anode composed of an LDC–NiO composite layer and a NiO layer. The second configuration was formed by applying an additional LDC layer between the LSGM electrolyte and the LSCF–LSGM cathode layers. LSGM tubes were fabricated by extrusion, and the anode, cathode, and buffer layers were deposited using dip coating. The effects of different paste formulations and sintering temperatures on the characteristics of the micro tubes, fabricated via extrusion techniques, were investigated. The electrochemical performances of the micro T-SOFCs with the two configurations were evaluated and compared.

2. Experimental procedure

2.1 Fabrication of the green electrolyte micro-tubes

In this study, electrolyte pastes were prepared from LSGM (Fuel Cell Materials; $d_{50} = 0.79\,\mu m$; BET surface area $= 4.31$ m^2/g), a binder (methyl cellulose, MC, Tsair Yu Technology), lubricant (Oil, Tsair Yu Technology), a surfactant, and D.I. water, at the weight ratios listed in **Table 1**. The mixtures were then aged in a plastic container for approximately 6 h. Workable pastes were extruded into micro-tubes by a custom-designed extrusion apparatus. The speed of the extrusion piston was set at 1.5 mm/s. After drying, the green micro-tubes with a diameter of 5 mm and a wall thickness of approximately 300 µm were cut to 50 mm in length. The electrolyte micro-tubes were then sintered at 1400, 1450, 1500, and 1550°C for 2 h (heating rate of 5 °C/min). Scanning electron microscopy (SEM, Joel JSM-6510LV) was used to examine the microstructures on the fractured surfaces of the micro-tubes. The density of the electrolyte micro-tubes was characterized using the water immersion (Archimedes) method, and the porosity was estimated. The flexural strengths of the LSGM micro-tubes with maximum densification were determined by third-point loading (SHIMADZU; AG-IC) and expressed as the modulus of rupture (MR) in psi (MPa). The force at the breaking point was recorded and used to calculate the flexural strength (σ_F) according to the following equation.6)

$$\sigma_F \frac{8FLD}{\pi(D^4 - d^4)} \qquad (1)$$

where F is the measured load at fracture, and L, D, and d are the length (30 mm) and the outer and inner diameters of the micro-tubes, respectively.

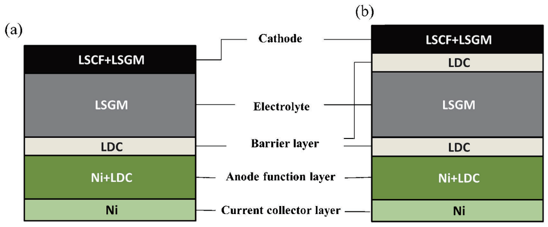

Fig. 1. Schematic drawing of the electrolyte-supported cell structure of micro T-SOFCs: (a) LSFC–LSGM/LSGM/LDC/Ni–LDC/Ni (Cell A); (b) LSFC–LSGM/LDC/LSGM/LDC/Ni–LDC/Ni (Cell B).

2.2 Coating of anode and cathode layers

SOFC single cells with two different configurations were prepared in this study, i.e., Cell A and Cell B, which are shown in **Fig. 1**. For Cell A, a thin LDC buffer layer was inserted between the anode and electrolyte layer to form an LDC–LSGM bi-layer electrolyte. For Cell B, a thin LDC buffer layer was introduced between the LSGM and the two electrodes to form a LDC–LSGM–LDC tri-layer electrolyte.

After cutting and drying, the green LSGM electrolyte micro-tubes were pre-fired at 1500°C before electrode coating. The formulations of slurries used for the different layers in this study are listed in **Table 2**. For Cell A, a thin buffer layer coating on the inner surface of the micro-tubes was fabricated through dip coating in a colloidal suspension of dispersed LDC particles

Table 2. Formulations of dip-coating slurries prepared in this study

Slurry	Functional powders (wt %)	Carbon powder (wt %)	Binder (wt %)	Solvent (wt %)
LDC	35.7	0	10.7	53.6
Anode NiO+LDC	37.7	3.8	11.3	47.2
NiO	40.3	0	19.4	40.3
Cathode LSGM+LSCF	43.9	0	21.0	35.1

(Fuel Cell Materials; $d_{50} = 0.58\,\mu m$; BET surface area = 4.41 m^2/g). For Cell B, both the inner and outer surfaces of the LSGM tubes were coated with a thin LDC buffer layer. The LDC-coated LSGM tubes were then fired at 1300°C for 1 h. Subsequently, the inner surfaces of the electrolyte tubes were then dip-coated with the anode slurry, as indicated in Table 2. NiO (SHOWA; $d_{50} = 0.8\,\mu m$; BET surface area = $2.80\,m^2/g$) and LDC powders were mixed at a volume ratio of 6:4. In addition, 30 vol.% carbon powders were added to produce sufficient porosity and to reduce the sintering mismatch with the electrolyte. The mixed powders were first ball-milled with ethanol and toluene (ratio of 3:2) for 2 h at a milling speed of 350 rpm. A binder (Ferro; B74600PF) was then added to the anode slurry and it was further ball-milled for 7 h. A current-collector layer of NiO was then dip-coated onto the surfaces of the anode NiO–LDC functional layer. After drying, the half-cells were co-sintered at 1350°C for 0.5 h in air.

After bi-layer anode coating and corresponding sintering, the LSGM–LSCF (Fuel Cell Materials; $d_{50} = 0.99\,\mu m$; BET surface area = $4.69\,m^2/g$) composite cathode was dip-coated onto the central portions of the outer surfaces of the micro-tubes in a suspension containing LSCF and LSGM powders. LSCF and LSGM powders were mixed at a volume ratio of 8:2. The mixed powders were ball-milled with ethanol and toluene (weight ratio of 3:2). After ball milling, the cathode slurry was poured into a container and dip-coated onto the outer surfaces of the electrolyte micro-tubes. After drying, the micro T-SOFCs with a green composite cathode were post-sintered at 1100°C for 2 h in air.

2.3 Characterization of the SOFC single cells

The cross-sectional microstructures of Cell A and Cell B were examined by SEM and energy dispersive spectroscopy (EDS). The electrochemical impedances and cell performances of the micro T-SOFCs were evaluated using an in-house setup with a tube furnace. For current collection, Ag wire was coiled around the outer cathode surface of the tubular cell. Nickel foam was curled and sealed on the inner anode surface of the tube using silver paste. The micro T-SOFCs were mounted at the end of an alumina tube with a sealant (Aremco products, Zirconia 885), and the temperature was controlled by a thermocouple located nearby. H_2 was introduced at a flow rate of 15 sccm to the anode side, and the reduction of the NiO at the anode was accomplished at 650°C over 1 h to promote good ohmic contact between the anode and the current collector. Cell voltage and power density as a function of cell current density were determined using a potentiostatic instrument (Jiehan ECW-5000) at temperatures from 650 to 800°C at an interval of 50°C. The fuel utilization of the micro T-SOFCs appeared to be greater than 55%, depending on the operating temperature. Impedance analysis was conducted using an electrochemical impedance analyzer (Jiehan IMS-3522Z) in the frequency range of 0.1 to 10^4 Hz.

3. Results and discussion

(a) Preparation of electrolyte micro-tubes

In order to minimize the thickness of the electrolyte, thus enabling it to operate at low temperature while still providing enough strength to maintain the mechanical integrity of the SOFC structure, the tubular electrolyte was fabricated to have an optimal thickness ranging from 220 to 300 µm after sintering. Commonly, the powder characteristics, organic additives, mixing procedure, and extrusion parameters all play important roles in the quality of the final extruded micro-tubes.[22),23)] Table 1 lists some of the formulations employed for the electrolyte pastes used to extrude the LSGM micro-tubes. Using identical mixing procedures, extrusion parameters, and LSGM powders, the effects of the organic additives on the characteristics of the extruded micro-tubes were investigated, and the corresponding results are presented in Table 1. It is evident that the properties of the green micro-tubes depend on the additive content to a great extent.

Extrusion of the LSGM paste containing less than 13.5 wt % water was not successful due to insufficient moisture. The optimal water content, which strongly depends on the particle size of the LSGM powders, was found to be 13.6–14.0 wt %. The results of this study suggest that the addition of at least 1.1 wt % MC to the LSGM powders is necessary to obtain an extrudable paste owing to the small particle size ($d_{50} = 0.79\,\mu m$) and large surface area ($4.31\,m^2/g$) of the LSGM powders. For the LSGM-1 paste, 0.9 wt % MC was not enough to completely cover the surfaces of the particles, resulting in non-smooth extrusion. The paste with excessive MC addition (LSGM-3 paste) gives rise to micro-tubes with acceptable smooth appearances but a low green density owing to the relatively high content of binder (1.27%). For the paste with 1.17 wt % MC (LSGM-2), micro-tubes with acceptable shapes and smooth surfaces were obtained. Furthermore, the oil content is a critical parameter in the extrusion process. The use of paste with insufficient oil (LSGM-4; 1.25%) leads to difficulties in extrusion and results in the extruded micro-tubes with rough surfaces, while excess oil (LSGM-5; 1.46%) typically produced micro-tubes with pinholes on their surfaces, and the tubes were elongated. The dispersant added to the paste is important for bridging the ceramic powders and the binder, thereby reducing the degree of agglomeration. The paste with insufficient surfactant (LSGM-6; 0.33 wt %) was found too dry and too hard for extrusion. This may be improved if more MC and oil are added. For the paste with 0.75 wt % surfactant, the characteristics of the micro-tubes are similar to those for the paste with 0.50 wt % surfactant. Overall, based on the above observation, an LSGM-2 paste containing 1.17 wt % MC, 1.33 wt % oil, 13.75 wt % water, and 0.5 wt % surfactant forms micro-tubes with the best characteristics, and this composition was chosen for all subsequent work.

(b) Characteristics of the sintered electrolyte micro-tubes

The densities of the green LSGM tubes sintered at 1400, 1450, 1500, and 1550°C were determined to be 6.24, 6.08, 6.26, and $5.98\,g/cm^3$, respectively, corresponding to 94.7, 92.6, 95.0, and 90.8% of the theoretical density ($6.59\,g/cm^3$). It should be noted that the LSGM micro-tubes collapse upon sintering at 1550°C, and the best densification was achieved at a sintering temperature of 1500°C. A photograph and an SEM micrograph of the LSGM micro-tubes sintered at 1500°C are shown **Fig. 2**. No physical defects are visible on the fractured surfaces. Tube walls with uniform thickness and smooth and glossy tube surfaces are observed. No pinholes and worm-shaped surface are evident. **Figure 3** shows the SEM micrographs of the fractured surfaces of the LSGM micro-tubes fired at 1400, 1450, 1500, and 1550°C. The SEM images indicate trans-granular fractures that cross the grains of the material and result in fairly smooth-looking fractures, which commonly occurs in microstructures in the absence of a second phase at the grain boundaries. The porosity of the

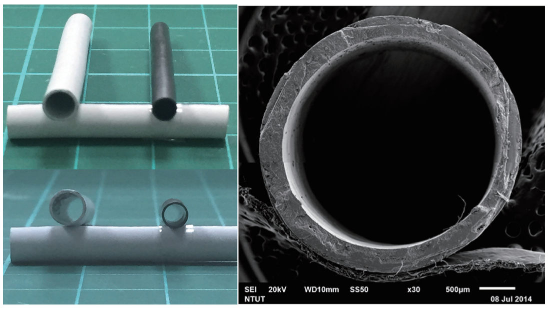

Fig. 2. Photograph and SEM micrograph of LSGM micro-tubes sintered at 1500°C.

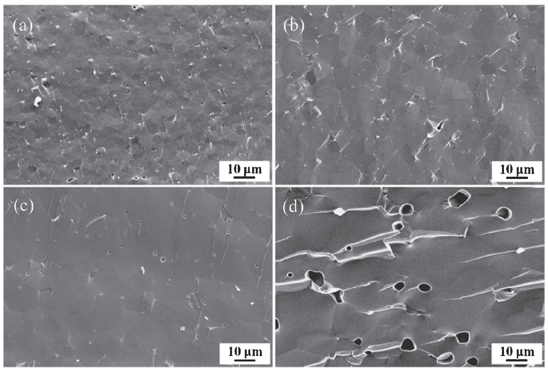

Fig. 3. SEM micrographs of as-fired surfaces of LSGM micro-tubes fired at (a) 1400°C, (b) 1450°C, (c) 1500°C, and (d) 1550°C.

microstructures decreases with increasing sintering temperature up to 1500°C. A dense microstructure with only few small pores (approximately 0.5 µm) that are scattered along the grain boundaries and triple points is formed. However, as the sintering temperature approaches 1550°C, large sized pores of approximately 5 µm are distributed on the microstructures. SEM studies on the as-sintered surfaces of the LSGM micro-tubes were also conducted, and microstructures with a uniform grain size are observed. The average grain size of the LSGM micro-tubes sintered at 1400, 1450, and 1500°C are 3.0, 6.2, and 8.0 µm, respectively, indicating the rapid increase of grain size with increasing sintering temperature.

The longitudinal and lateral shrinkage of the micro-tubes sintered at 1500°C are approximately 24 and 27%, respectively, and the thickness of the tube wall decreases by 33%. Typical dimensions of the LSGM micro-tubes with an initial length of 21.65 mm, an initial outer diameter of 4.57 mm, and an initial tube wall thickness of 0.45 mm after sintering at 1500°C for 2 h are 16.42 mm length, 3.37 mm diameter, and a wall thickness of 0.3 mm. The flexural strength of the LSGM micro-tubes sintered at 1500°C was determined to be approximately 144 MPa using Eq. (1), which is similar to the values observed for bulk LSGM materials.[24),25)] The flexural strength is high enough for SOFC applications, even though it is smaller than that of $Zr_{0.8}Sc_{0.2}O_{2-\delta}$ micro-tubes with similar dimensions (approximately 190 MPa).[6)]

(c) Characteristics of SOFC single cells with bi-layer and tri-layer electrolytes

Figure 4 shows the typical optical images of Cell A (LSFC–LSGM/LSGM/LDC/Ni–LDC/Ni) after LSGM–LSCF composite cathode fired onto the outer surfaces of the tubes. The final dimensions of the electrolyte-supported micro T-SOFCs are an outer diameter of 3.3 mm, an inner diameter of 3.0 mm, and a cathode length of 5.1 mm, which represents an effective cell area of 0.53 cm^2.

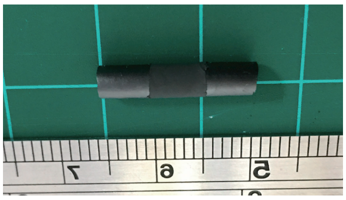

Fig. 4. Optical image of Cell A (LSFC–LSGM/LSGM/LDC/Ni–LDC/Ni) micro T-SOFC.

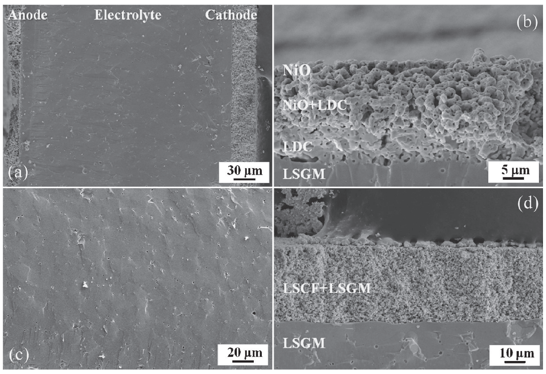

Fig. 5. SEM micrographs of the cross-section fracture surfaces of (a) the entire cell, (b) region across the electrolyte/bilayer anode interface, (c) electrolyte layer, and (d) region across the electrolyte/cathode interface of Cell A, after electrochemical measurement.

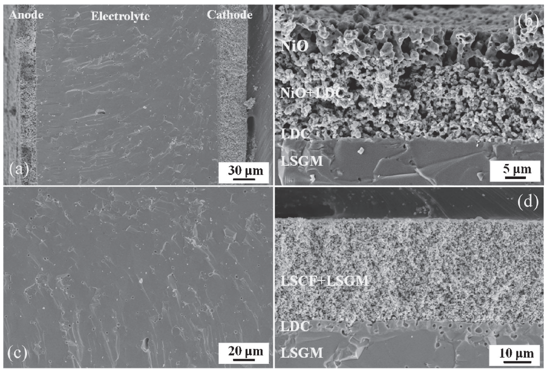

Fig. 6. SEM micrographs of the cross-section fracture surfaces of (a) the entire cell, (b) region across the electrolyte/bilayer anode interface, (c) electrolyte layer, and (d) region across the electrolyte/cathode interface of Cell B, after electrochemical measurement.

Figures 5 and **6** show cross-sectional SEM micrographs of the fractured surfaces of Cell A and Cell B after the electrochemical measurement. Uniform and dense LSGM electrolyte layers for Cell A and Cell B with thicknesses of 288 and 245 µm, respectively, are observed, as shown in Figs. 5(a) and 6(a). They appear to be rather dense with no interconnecting pores or cracks [Figs. 5(c) and 6(c)], suggesting the absence of gas penetration across the electrolyte from one electrode to the other during operation. A LDC layer with a thickness of approximately 8 µm is situated between the electrolyte and anode layers in Cell A, while two LDC layers with thicknesses of nearly 2 µm are formed between the electrolyte and anode, and layers with thicknesses of about 4 µm are formed between the electrolyte and cathode, demonstrating good adherence to the LSGM tube, although some micro-pores are present in the layers and at the interfaces. Further reduction in the thickness of the LDC layer was not considered in this study because the thickness of the electrolyte layer in electrolyte-supported T-SOFCs falls generally in the range of a few hundredths to a few thousandths of a micrometer; thus, the effect of such a thickness on the ohmic resistance of the cell is inconsequential. Both the cathode and anode electrodes show a typical porous microstructure and display an excellent interface attached to the electrolyte layer. The high-magnification images of the anodes of Cell A and Cell B indicate total thicknesses of approximately 13 and 24 µm, respectively, as shown in Figs. 5(b) and 6(b). The outer current-collector layer contains a skeleton of porous Ni granular particles of approximately 2 µm in size and with an interconnecting porosity of 3 to 10 µm, while the inner anode functional LDC–Ni layer presents an interconnecting porosity of 1 to 3 µm. SEM micrographs showing the interfaces of the cathode and the electrolyte for Cell A and Cell B are presented in Figs. 5(d) and 6(d), in which the LSCF–LSGM composite cathode layers show a thickness of approximately 33 and 35 µm, respectively, and are well adhered to the LSGM electrolyte tubes. The high-magnification microstructure of the composite cathode indicates an average pore size of approximately 1 µm. In order for a SOFC to maintain good performance, both the anode and cathode need to have a well-constructed porous microstructure.[25),26)] As previously reported in the literatures, a chemical reaction between LSGM and the NiO-containing anode to produce second phases of $LaNiO_3$ and La_2NiO_4 is observed, which destabilize the perovskite structure and thus degrade the performance and durability of the cell.[18),27)] Upon the insertion of the LDC buffer layer, the results of EDS studies indicate that no detectable inter-diffusion of the NiO and LSGM across the interfaces occurs, and no interfacial reaction zone is detected in this study. The microstructure of Cell A is similar to that of Cell B, except for the bi-layer LDC/LSGM electrolyte in Cell A and the tri-layer LDC/LSGM/LDC electrolyte in Cell B. The variation in the total anode thickness between Cell A and Cell B is due to their different coating procedures, which were confirmed in this study to have an insignificant effect on their electrochemical properties. This finding is consistent with observations reported in the literature, i.e., that the polarization loss from the anode side is trivial enough to be ignored when compared to its counterpart from the cathode side.[17),19),28)]

Figures 7(a) and 7(b) present the electrochemical impedance spectra of Cell A and Cell B at 650, 700, 750, and 800°C. **Table 3** lists the ohmic resistance (R_o) values representing the highest frequency intercept on the real axis, and the polarization resistance (R_p) values representing the distance between the intercepts of the lowest and the highest frequencies on the real axis.[4),28)] Both R_o and R_p decrease with increasing measurement temperature, since the ionic conductivity of the LSGM increases with rising temperature.[24)] The ohmic resistances of Cell B are slightly larger than those of Cell A at all temperatures, mainly because of the interfacial resistance, which is caused by differences between the interfacial resistances of LSGM/LSCF–LSGM and the sum of the interfacial resistances of LSGM/LDC and LDC/LSCF–LSGM at different temperatures. However, compared to Cell A, the insertion of the LDC layer between the LSGM electrolyte and the LSCF–LSGM composite cathode in Cell B causes insignificant change in polarization resistance at the operating temperatures investigated. The total resistance (R_t) values ($= R_o + R_p$) of Cell B with the LDC/LSGM/LDC tri-layer electrolyte are slightly higher than those of Cell A with the LDC/LGGM bi-layer electrolyte at all temperatures except 750°C. Considering that the total electrolyte thickness of the Cell B (251 µm; 245 µm for LSGM and 6 µm for the two LDC layers) is less than that of the Cell A (296 µm; 288 µm LSGM and 8 µm LDC), it is expected that the difference in R_t values between Cell A and Cell B will be even larger if their total electrolyte thickness are the same.

Figure 8 shows the *I–V* curves and corresponding power densities of Cell A and Cell B at different temperatures. The OCVs of Cell A and Cell B are 1.08 and 1.06 V, respectively, at all temperatures, which are close to the theoretically predicted value, indicating dense electrolyte layers in the cells and good sealing during measurement. The area specific resistance (ASR) values, as derived from the initial slopes of the *I–V* curves, are listed in Table 3. The calculated ASR values at different temperatures are close to the R_t values. The MPDs of Cell A are 0.25, 0.35, 0.43, and 0.47 W cm^{-2} at 650, 700, 750, and 800°C, respectively, while those of Cell B are 0.23, 0.33, 0.42, and 0.41 W cm^{-2}, respec-

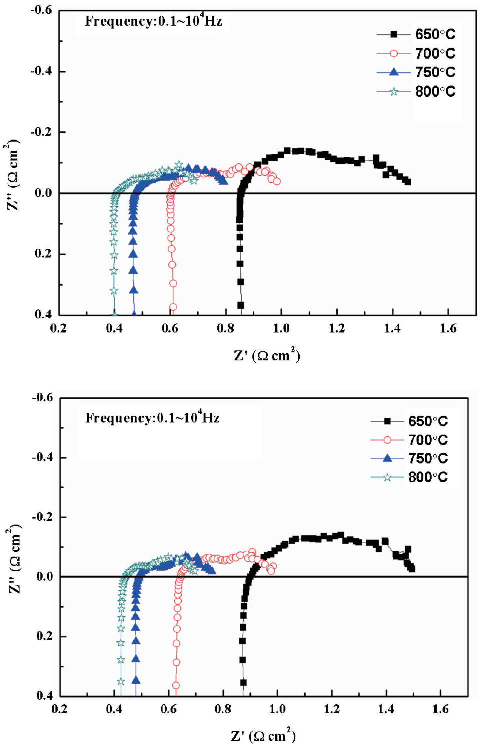

Fig. 7. Impedance spectra of (a) Cell A and (b) Cell B at different temperatures.

Table 3. Ohmic resistance (R_o) and polarization resistance (R_p) values of Cell A and Cell B obtained from the impedance spectra shown in Fig. 7 and the area specific resistance values of the cells (ASR_{cell}) calculated from the initial slopes of the *I–V* curves shown in Fig. 8

Temperature	Cell A					Cell B				
	R_o (Ω cm²)	R_p (Ω cm²)	$R_t = R_0 + R_p$	ASR_{cell} (Ω cm²)	Power density (W/cm³)	R_o (Ω cm²)	R_p (Ω cm²)	$R_t = R_0 + R_p$	ASR_{cell} (Ω cm²)	Power density (W/cm³)
650°C	0.86	0.60	1.46	1.46	0.25	0.90	0.60	1.50	1.57	0.227
700°C	0.61	0.38	0.98	0.95	0.35	0.65	0.33	0.98	0.90	0.331
750°C	0.47	0.32	0.79	0.79	0.43	0.49	0.27	0.76	0.68	0.415
800°C	0.41	0.28	0.69	0.69	0.47	0.44	0.25	0.70	0.67	0.412

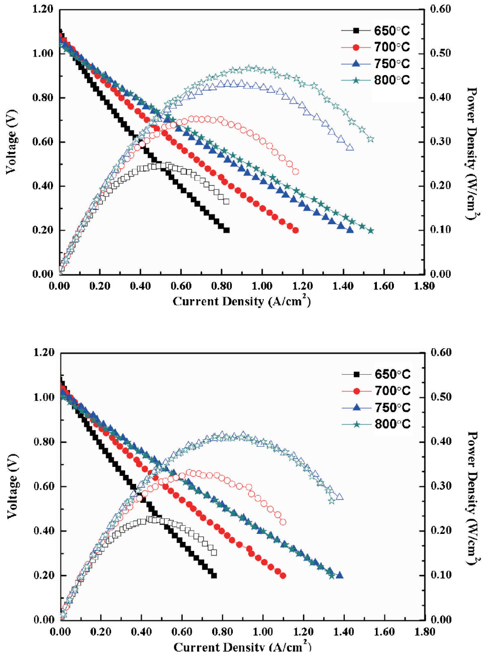

Fig. 8. *I–V* curves and the corresponding power densities of (a) Cell A and (b) Cell B at different temperatures.

tively. The former exhibits larger MPDs at all temperatures compared with those of the latter. This may be due to the facts that Cell A exhibits a slightly higher OCV and smaller R_t, as shown in the impedance spectrum (Table 3).

Based on the results of this study, the LSGM-supported SOFC single cells with an LDC/LSGM bi-layer electrolyte work apparently better than their counterparts with the LDC/LSGM/LDC tri-layer electrolyte, in terms of cell performance. The insertion of an additional LDC layer to cathode/electrolyte interface seems to have no improvement to the cell performance. Compared with those obtained in previous studies that used ScSZ and GDC–ScSZ as electrolytes for micro T-SOFCs with similar designs6),12) and which exhibited MPDs of approximately 0.25 W cm^{-2}, the micro T-SOFC single cell with the 210-µm ScSZ electrolyte has to be operated at 900°C, and that with the GDC (285-µm)–ScSZ (8 µm) bi-layer electrolyte has to be operated at 700°C. However, Cell A with the LSGM (288 µm)–LDC (8 µm) bi-layer electrolyte can be operated at approximately 650°C. Thus, the advantage of using LSGM as an electrolyte for micro T-SOFC single cell is evident.

4. Conclusion

LSGM-supported micro T-SOFCs containing a LDC/LSGM bi-layer electrolyte or a LDC–LSGM–LDC tri-layer electrolyte were fabricated. The ohmic resistances of Cell B were slightly higher than those of Cell A at all temperatures investigated, mainly because of the interfacial resistance. However, compared to the case of Cell A, the insertion of the LDC layer between the LSGM electrolyte and the LSCF–LSGM composite cathode in Cell B caused a slight decrease in polarization resistance. Owing to the facts that Cell A exhibits a slightly higher OCV and smaller R_t values, the MPDs of Cell A are 0.25, 0.35, 0.43, and 0.47 W cm^{-2} at 650, 700, 750, and 800°C, respectively, which are slightly larger than those of Cell B, reported as 0.23, 0.33, 0.42, and 0.41 W cm^{-2}, respectively.

Acknowledgement This work was supported by the 2nd Polish-Taiwanese/Taiwanese-Polish Joint Research Project DZP/PL-TW2/6/2015 - Innovative Solid Oxide Electrolyzers for Storage of Renewable Energy granted by the National Centre for Research and Development of Poland and Ministry of Science and Technology of Taiwan.

References

1) O. Yamamoto, *Electrochim. Acta*, 45, 2423–2435 (2000).
2) V. Lawlor, S. Griesser, G. Buchinger, A. G. Olabi, S. Cordiner and D. Meissner, *J. Power Sources*, 193, 387–399 (2009).
3) M. Torrell, A. Morata, P. Kayser, M. Kendall, K. Kendall and A. Tarancon, *J. Power Sources*, 285, 439–448 (2015).
4) K. S. Howe, G. J. Thompson and K. Kendall, *J. Power Sources*, 196, 1677–1686 (2011).
5) S. M. Wu and K. T. Lee, *J. Ceram. Process. Res.*, 17, 672–675 (2016).
6) W. S. Hsieh, P. Lin and S. F. Wang, *Int. J. Hydrogen Energy*, 38, 2859–2867 (2013).
7) T. Suzuki, Y. Funahashi, T. Yamaguchi, Y. Fujishiro and M. Awano, *Electrochemical and Solid-State Letters*; 10, 8, 177-179 (2007).
8) T. Liu, Y. Wang, C. Ren, S. Fang, Y. Mao and F. Chen, *J. Power Sources*, 293, 852–858 (2015).
9) X. Zhang, B. Lin, Y. Ling, Y. Dong, G. Meng and X. Liu, *Int. J. Hydrogen Energy*, 35, 8654–8662 (2010).
10) M. Morales, M. E. Navarro, X. G. Capdevila, J. J. Roa and M. Segarra, *Ceram. Int.*, 38, 3713–3722 (2012).
11) A. Faes, A. Nakajo, A. Hessler-Wyser, D. Dubois, A. Brisse, S. Modena and J. Van herle, *J. Power Sources*, 193, 55–64 (2009).
12) W. S. Hsieh, P. Lin and S. F. Wang, *Int. J. Hydrogen Energy*, 39, 17267–17274 (2014).
13) C. Ren, Y. Gan, M. Lee, C. Yang, F. He, Y. Jiang, G. Dong, R. D. Green and X. Xue, *J. Electrochem. Soc.*, 163, 1115–1123 (2016).
14) B. C. H. Steele, *Solid State Ionics*, 129, 95–110 (2000).
15) D. Lee, J. H. Han, Y. Chun, R. H. Song and D. R. Shin, *J. Power Sources*, 166, 35–40 (2007).
16) K. Hosoi, J. E. Hong, T. Sakai, S. Ida and T. Ishihara, *J. Ceram. Soc. Japan*, 123, 182–186 (2015).
17) K. Hosoi, T. Sakai, S. Ida and T. Ishihara, *J. Electrochem. Soc.*, 162, 1379–1383 (2015).
18) S. M. Yu and K. T. Lee, *J. Ceram. Process. Res.*, 17, 672–675 (2016).
19) L. Zhang, J. Xiao, Y. Xie, Y. Tang, J. Liu and M. Liu, *J. Alloys Compd.*, 608, 272–277 (2014).
20) G. Ju, K. Reifsnider, X. Huang and Y. Du, *J. Fuel Cell Sci. Technol.*, 35, 35–42 (2004).
21) H. Sun, Y. Chen, F. Chen, Y. Zhang and M. Liu, *J. Power Sources*, 301, 199–203 (2016).
22) F. Händle, *Springer Berlin Heidelberg New York*, 327 (2010).
23) A. Mat, M. Canavar, B. Timurkutluk and Y. Kaplan, *Int. J. Hydrogen Energy*, 41, 10037–10043 (2016).
24) M. Morales, J. J. Roa, J. Tartaj and M. Segarra, *J. Eur. Ceram. Soc.*, 36, 1–16 (2016).
25) K. Suna, J. Zhang, T. Jiang, J. Qiao, W. Sun, D. Rooney and Z. Wang, *Electrochim. Acta*, 196, 487–495 (2016).
26) K. Kendall and M. Palin, *J. Power Sources*, 71, 268–270 (1998).
27) Y. Lin and S. A. Barnett, *Electrochem. Solid-State Lett.*, 9, A285–A288 (2006).
28) Y. Du, N. M. Sammes, G. A. Tompsett, D. Zhang, J. Swan and M. Bowden, *J. Electrochem. Soc.*, 150, A74–A78 (2003).
29) Z. Bi, B. Yi, Z. Wang, Y. Dong, H. Wu, Y. She and M. Cheng, *Electrochem. Solid-State Lett.*, 7, A105–A107 (2004).
30) F. Bozza, R. Polini and E. Traversa, *Electrochem. Commun.*, 11, 1680–1683 (2009).
31) J. H. Wan, J. Q. Yan and J. B. Goodenough, *J. Electrochem. Soc.*, 152, A1511–A1515 (2005).